CCFE
CULHAM CENTRE FOR FUSION ENERGY

UK Atomic Energy Authority

UKAEA-CCFE-CP(23)24

W.G. Fuller, S. Allan, B, Hnat, N.R. Walkden

Optimising the Design of a New Turbulence Probe for MAST-U

Optimising the Design of a New Turbulence Probe for MAST-U

W.G. Fuller, S. Allan, B, Hnat, N.R. Walkden

This paper has been submitted to
47th IOP Plasma Physics Conference, London, UK 6-9 April 2021

Langmuir Probe Technique for Velocity Distribution Measurements in Tokamak Scrape Off Layer Plasmas

W. G. Fuller[1,2], S. Allan[2], B. Hnat[1] and N. R. Walkden[2]

[1] Centre for Fusion, Space and Astrophysics, Physics Department, University of Warwick UK

[2] UKAEA, Culham Science Centre, Abingdon, Oxfordshire, OX14 3DB, UK

E-mail: b.hnat@warwick.ac.uk

Abstract. We explore a Langmuir probe diagnostics technique for measuring the radial velocity distribution of synthetic density filaments generated by the stochastic model with parameters relevant to filament dynamics in the scrape off layer of MAST-U tokamak plasmas. This technique will be incorporated into the optimised design for a probe to be installed on MAST-U. The measured radial velocity distributions reproduce distributions of the model for low intermittency, narrower filament widths and typical systemic noise test cases. We show that for a probe separation of 10mm, the measured distribution fitted the input distribution better than the other probe separations we tested. The analysis suggests that this measurement technique may be a useful tool to analyse radial transport via filament motion in the tokamak scrape off layer.

1. Introduction

Mega ampere spherical tokamak upgrade (MAST-U) is the culmination of a substantial upgrade of the previous device, MAST. This upgrade includes a ground-breaking advanced divertor configuration aiming to reduce exhaust heat flux incident on the divertor surfaces [1,2]. To facilitate this, the advanced divertor has an extended divertor region with additional magnetic coils allowing the machine to create novel divertor field geometries such as x-divertor [2, 3], super-x [1, 4, 5], and snowflake [1, 2, 6] amongst others. The combination of novel field geometries and the extended divertor region should allow MAST-U to demonstrate enhanced access to detachment, through high neutral closure and larger total flux expansion [1, 5, 7]. Radial scrape off layer (SOL) transport plays a key role in determining flux densities into and within the divertor [1,8]. This transport is known to be mediated in part by coherent structures called filaments [9] and measurement of filament radial velocity will be an important aspect of characterising the MAST-U exhaust region [2, 8].

The SOL in a tokamak is the layer of plasma that lies outside the last closed flux surface; it is very turbulent with many plasma parameter fluctuations existing in a broad range of length scales. An important transport of heat [9,10] and particles are fast moving density profiles known as either filaments, blobs, or intermittent plasma objects [9–21]. For consistency we will refer to them as filaments. Filaments are present in L-mode and in H-mode plasmas, during and between ELMs [12, 15, 16, 19, 20, 22], however in this paper the work we have done concerns only L-mode filaments. Filaments are responsible for the majority of the particle transport [2, 12, 13, 16–18, 18–20, 23], carrying particles to the far SOL where there is potential to damage the first wall [3, 12, 24, 25] and a greater understanding of their dynamics is fundamental l for future burning plasma fusion devices like ITER, DEMO and STEP. Filaments have been observed and studied for many years [9, 14–17, 21, 22, 26], a comprehensive review of experiment and theory is provided by D. A. D'Ippolito, J. R. Myra and S. J. Zweben [9].

The MAST-U reciprocating probe (RP) system, situated at the midplane, has a suite of interchangeable probe heads including: a Mach probe [27], a Gundestrup/Ball-pen probe [28, 29] and a Retarding Field Analyser (RFEA) [10, 30, 31]. The RP has a maximum extension of 10cm [27] and operates inside the plasma SOL reciprocating into and out of the plasma to a maximum depth between 1cm – 2cm at a velocity of 0.9 $\mathrm{m\,s^{-1}}$, the probe head typically interacts with the plasma edge for less than 150 ms [27]. Of the probe heads available to MAST-U, none are specifically designed for turbulence studies. The Mach probe is designed to measure fluctuations in current saturation and in combination with D_α measurements, the velocity of these fluctuations can be calculated [27]. The Gundestrup is used to measure the ion saturation current and floating potential which can be used to calculate the electron density (n_e) and temperature (T_e) [28]. The Ball-pen probe is designed to directly measure the plasma potentialwhich can lead to more accurate electron temperature calculations than the Gundestrup probe [2, 29]. The RFEA probe head measures plasma ion characteristics

such as ion temperature and density [30,31]. Whilst individually these probe heads may be used for turbulence studies, for more comprehensive studies requiring a multitude of measurements, you would need to cease operations and swap out the probe head each time. We aim to create a single probe head that is designed to capture as many different turbulence effects as possible. Thus, providing a wealth of probe data to fuel a multitude of SOL turbulence studies for future users. With the new divertor capabilities comes a need to study how these alternate configurations affect the scrape-off-layer (SOL) dynamics, for instance how this will affect the filament transport mechanisms. It is imperative to explore filaments in these scenarios [1, 2, 8, 12, 13, 18, 20] to enhance our understanding, motivating us to develop a probe technique targeted at measuring filament characteristics to add to the new turbulence probe we are designing. To best design a turbulence probe for the MAST-U RP system we settled on a synthetic approach in which we performed simulations with a synthetic probe array design to assess the layout and tailor the design for optimal data collection of specific turbulent features.

To aid in the design of a turbulence probe, the synthetic probe requires numerous techniques to acquire filament properties. To generate the filaments, we used a stochastic framework introduced by O. E. Garcia [32] that was extended by F. Militello and J. T. Omotani [33–35] (henceforth referred to as the MO model) in which a stochastic model for filament dynamics in the SOL at the midplane was used to generate a synthetic plasma density signal used as a surrogate for probe data. The model is ideal for our use due to the large parameter space flexibility and low computational costs [33–36]. The parameters we used (shown in table 1) in the simulations are relevant for MAST and therefore a reasonable estimate for MAST-U as discussed in section 3.

In this paper we explore a simple array of three probes utilising their relative geometry to calculate a radial velocity distribution (which we discuss in section 2) for the filaments generated by the model discussed in section 3. In sections 4 and 5 we then present and evaluate the results of measuring radial velocity distributions produced by the stochastic model and finish on our conclusions of the study in section 6.

2. Probe Velocity Technique

In probe arrays designed for RP like systems, probes are carefully designed such that the probe collection area is less than the Debye sheath to keep plasma perturbation to a minimum. Probes typically have radii less than 1mm and the probe tips typically protrude into the plasma by 1-3mm [17, 18, 21, 27]. Radial offsets must be aligned carefully to also minimise perturbations, offsets of 10mm like we present are not uncommon [21, 37]. The radial velocity is an important property of filaments defining their radial transport. The velocity can be impacted by plasma properties [11,12,18,26] such as the plasma collisionality as suggested by others [14, 18, 38–41]. In what follows, we consider an array of three probes: probes 2 and 3 have a poloidal separation only, while probe 1 is radially offset from 2, 3 as shown in figure 1a. We can utilise this to decouple velocity measurements into their radial and poloidal components. Using

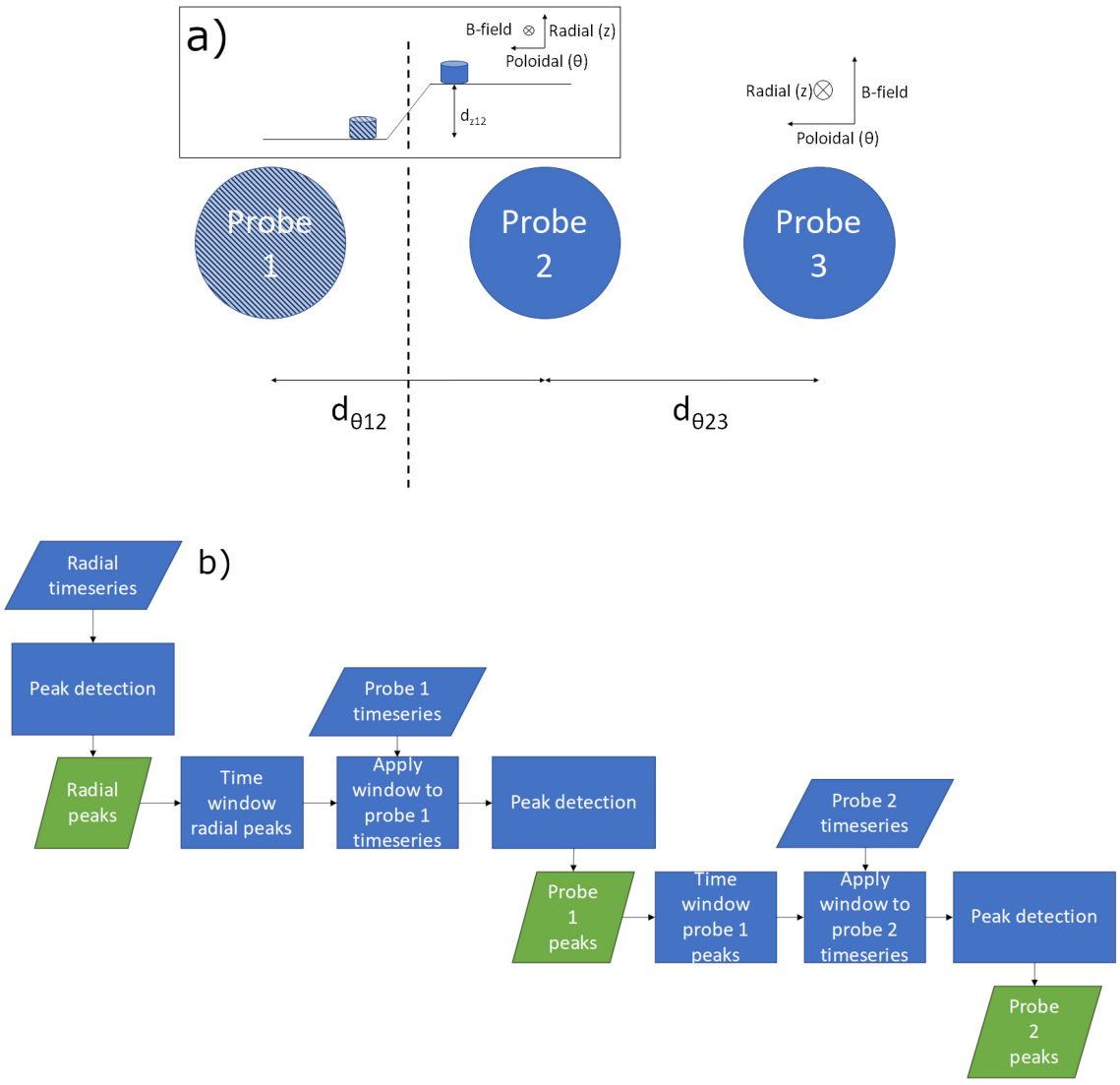

Figure 1: (a) is a schematic showing the layout and separation between the three Langmuir probes used in this paper. (b) is a flow chart describing the peak finding algorithm used.

simple geometry, assuming the filaments width is sufficiently large, and the velocity is orientated such that all three pins are crossed, we calculate the following velocities shown as in equations (1), (2), and (3).

Table 1: This is a table for the default parameters used in the MO model filament simulations.

Parameter	Value	Range	Description
`R_distribution`	Lognormal (Nfils, $\sigma = 0.4, \mu = 0$)	1.32 – 1.34 m	Distribution of filaments in the radial direction
`Tor_distribution`	Uniform (Nfils)	-1.32π – 1.32π m	Distribution of filaments in the toroidal direction
`dR/dtor_distribution`	Lognormal (Nfils, $\sigma = 0.4, \mu = 0$)	0.005 – 0.02 m	Distribution of filament widths in the radial and toroidal directions
`vR_distribution`	Lognormal (Nfils, $\sigma = 0.4, \mu = 0$)	100 – 1500 $m\,s^{-1}$	Distribution of filament radial velocities
`vtor_distribution`	Uniform (Nfils)	-500 – 2000 $m\,s^{-1}$	Distribution of filament toroidal velocities
`amp_distribution`	Exponential (scale = 1)	Nfils	Distribution of filament amplitudes
`spawn_distribution`	Uniform (Nfils)	0 – 0.1 s	Distribution of filaments in time
`Nfils`	200 000		Number of filaments to spawn
`dt`	1 e-6 s		Time between each step
`nt_evolve`	1000		Number of steps to evolve each filament
`drainagetime`	2.5 e-4 s		How quickly filament amplitudes decrease
`fwCrit`	1		Inertial sheath limited transition width
`divCol`	1		Normalised plasma resistivity integrated along B-field

$$v_\theta = \frac{t_3 - t_2}{d_{\theta_{2\,3}}} \tag{1}$$

$$v_{1\,2} = \frac{t_2 - t_1}{(d^2_{\theta_{1\,2}} + d^2_{z_{1\,2}})^{1/2}} \tag{2}$$

$$v_R = \sqrt{v^2_{1\,2} - v^2_\theta} \tag{3}$$

Here v_θ is the poloidal velocity, $v_{1\,2}$ is the velocity between the radially offset probe 1 and probe 2, and v_R is the total radial velocity. $t_{1,2,3}$ is the time of the peak of the filament for probes 1, 2 and 3. $d_{\theta_{2\,3}}$ is the poloidal distance between probes 2 and 3, $d_{\theta_{1\,2}}$ is the poloidal distance between probe 1 and 2, $d_{z_{1\,2}}$ is the radial distance between probe 1 and probe 2. Figure 1a is a schematic representation of the probe layout. We translated the probe layout from a vertical radial, poloidal coordinate system at the midplane onto the horizontal radial, toroidal midplane for the model, we found the field lines coincident with the probe positions and, using a field line tracing code like in [8,12], we traced the magnetic field onto the midplane and used the radial and toroidal coordinates to extract data from the model.

3. Stochastic Model of Filaments

The MO model generates a set of 'filaments' with randomly sampled parameters which are moved at constant velocity across a radial-toroidal box, with amplitude decreasing in time. We used a gaussian waveform to represent filaments in both the radial and toroidal directions. Unless otherwise stated, the default parameters used are shown in table 1. These default values are relevant for MAST L-mode plasmas and therefore a reasonable estimate for MAST-U too. The measured filament widths are typically around 2cm [2, 12, 20, 42], however we also ran a 50% reduced size scenario as discussed by Harrison et al [2] and observed by Thornton et al [8] to test the potential effect of smaller filament widths in the divertor region on the technique. Filament velocities vary from around 100-1500 $\mathrm{m\,s^{-1}}$ radially and up to 2000 $\mathrm{m\,s^{-1}}$ toroidally [2, 12, 15, 20, 42].

The simulations output as timeseries data for the measured density at each of the probe positions. These timeseries are fed into the SciPy `find_peaks` function with a minimum prominence of 2.5 standard deviations (σ). We set this prominence value as such even though all the peaks in the noiseless simulation timeseries will be filaments, to keep in line with typical experimental methods [17, 18, 23, 36, 41, 43]. The peaks must be detected within a time window of 0.12 ms (for a probe separation of 10mm corresponds to a minimum velocity of 83 $\mathrm{m\,s^{-1}}$) on all three probes. On each probe detected peaks amplitudes cannot differ by more than 10%. This ensures that only peaks detected in all three probe signals are used in the velocity calculations. Figure 1b is a flowchart to help visualise the process. From each filament detected on all three probes, the radial velocity is calculated as described in equations (1), (2), and (3) with t as the time of each filament peak detected.

4. Results

Intermittency can be characterised from a probability distribution function (PDF) and calculating the 4^{th} order moment, kurtosis [9]. The kurtosis (K) is a measure of flatness of the distribution, Large K values imply longer tails of the PDF hence lower intermittency. The intermittency of timeseries measured in the tokamak SOL varies radially, from low near the separatrix to high in the far SOL. For a fixed time window, intermittency strongly affects the number of filaments detected by the probes. We test our detection algorithm using simulation data with 200 000, 20 000, and 500 filaments corresponding to low, medium, and high intermittency. Figure 2 shows that as the intermittency decreases, we observe more peaks. We detected 182 filaments for the low intermittency case, 65 filaments for the medium case and 9 filaments detected in all three probes for the high intermittency case. Figure 3 presents the input and measured radial velocity PDF with the calculated root mean squared (RMS) error, the kurtosis calculated for the low, medium, and high intermittencies are K = 31.0, k= 10.33 and K = -1.82. All of the PDFs were calculated with a bin size of 20. From the figure we can see that the low intermittency case matches reasonably well to the input distribution and

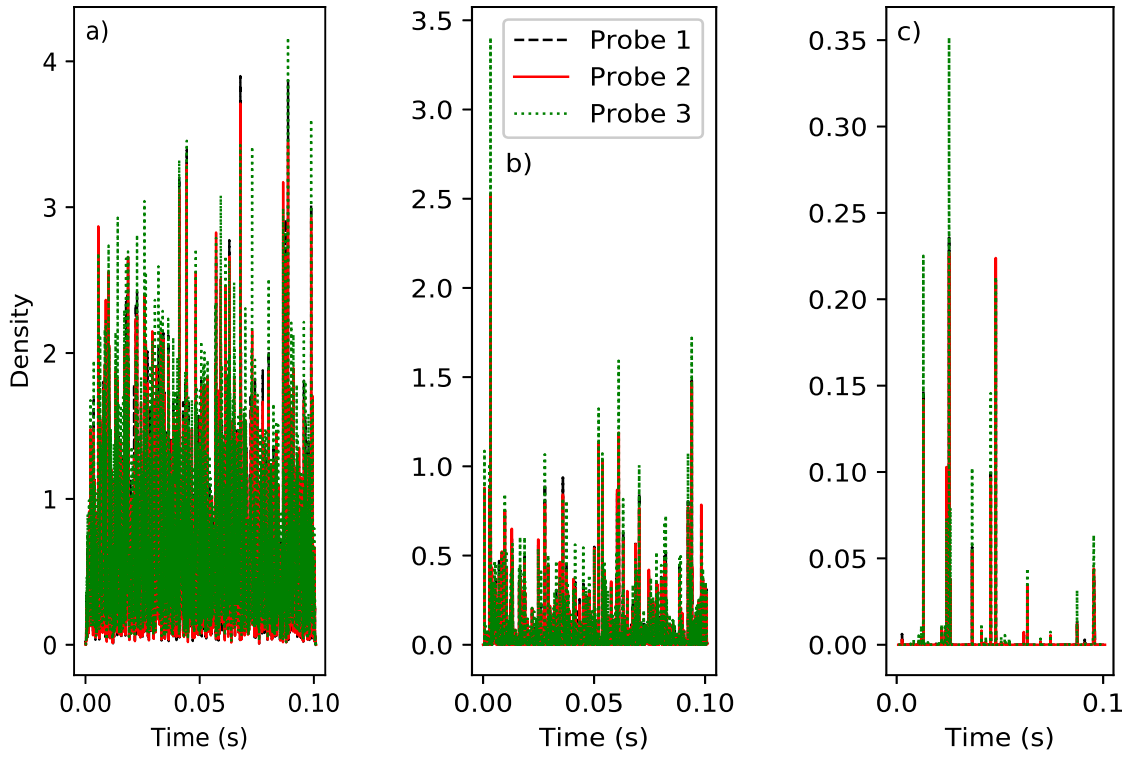

Figure 2: Left (a) is a low intermittency case with 200 000 filaments spawned and 182 filament peaks detected 2.5σ above the background for all three probes. Centre (b) is the medium intermittency case with 20 000 filaments spawned and 65 filaments detected in all three probes. Right (c) is the high intermittency case with 500 filaments spawned and 9 detected in all three probes.

has an RMS of 7.44×10^{-3}. The shape of the medium case can be seen though is less well resolved, and it has an RMS of 5.96×10^{-2}. We also ran another medium intermittency simulation with 200 000 filaments for 1 second (10 times the previous simulation time) shown in figure 3c to generate a comparable number of filaments at lower intermittancy, 612 peaks were detected and K = 32.19, the RMS error is an improvement on figure 3b with an RMS error of 2.35×10^{-2}. This is similarly well resolved compared to figure 3a indicating that the resolution of the distribution is purely statistical, and not related to the intermittency of the signal. Finally for the high intermittency case no fit to the PDF is possible as only nine filaments were detected – the RMS value of 7.02×10^{-2} is comparable to the PDF.

We averaged the radial velocity PDFs, shown in figure 4, over 10 runs for each intermittency test case, keeping all other parameters the same to demonstrate the statistical variation that occurs due to the stochastic nature of the model. In the figure for the low intermittency case, the average and a majority of the maxima are contained within the average input distribution, the medium case follows the general trend, and the high intermittency case suffers from a lack of statistically significant

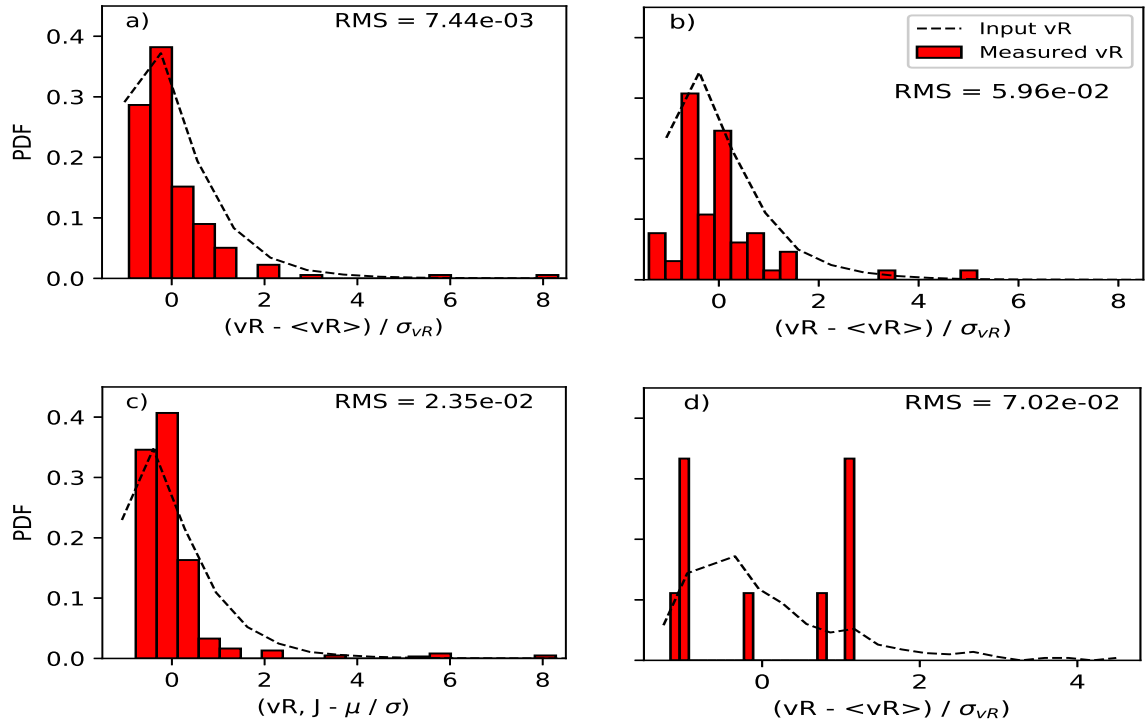

Figure 3: The input is the black line and red bars arethe measured radial velocity probability distributions for the three intermittency cases; top left (a) is low, right (b) is medium, bottom left (c) is low intermittency with 200 000 filaments, and bottom right (d) is the high intermittency. The RMS error is calculated for the each case.

filament population. From these averaged runs we calculated a percentage error from the maximum and minimum values compared to the mean and have applied these for the corresponding intermittency to the subsequent analyses.

To see how the velocity technique performs with noise, we added random gaussian noise to the low intermittency test case such that the signal to noise ratio (SNR) in decibels (dB) was 30 dB and 20 dB respectively. This corresponds to 0.1% and 1% added random gaussian noise to the reference signal. Figure 5 shows these compared to the noiseless low intermittency case and the input radial velocity distribution. To process the noisy signal first we ran a windowed smoothing function with a window size of 5 μs. For 30dB the distribution shape follows a similar trend to the noiseless measured case. The PDF in the case with a SNR of 20dB also follows a similar shape to the 30dB distributionand therefore the noiseless case.

We reduced the filament width by 50% from 5-20mm to 2.5-10mm for the low intermittency case in order to assess the effect of narrower filaments on our measurement technique. Figure 6 demonstrates that the ability for the technique to measure the radial velocity distribution is unaffected.

In order to assess the impact of the probe array layout, we adjusted the relative positions of the three probes as shown in figure 7, and figure 8. The default case is

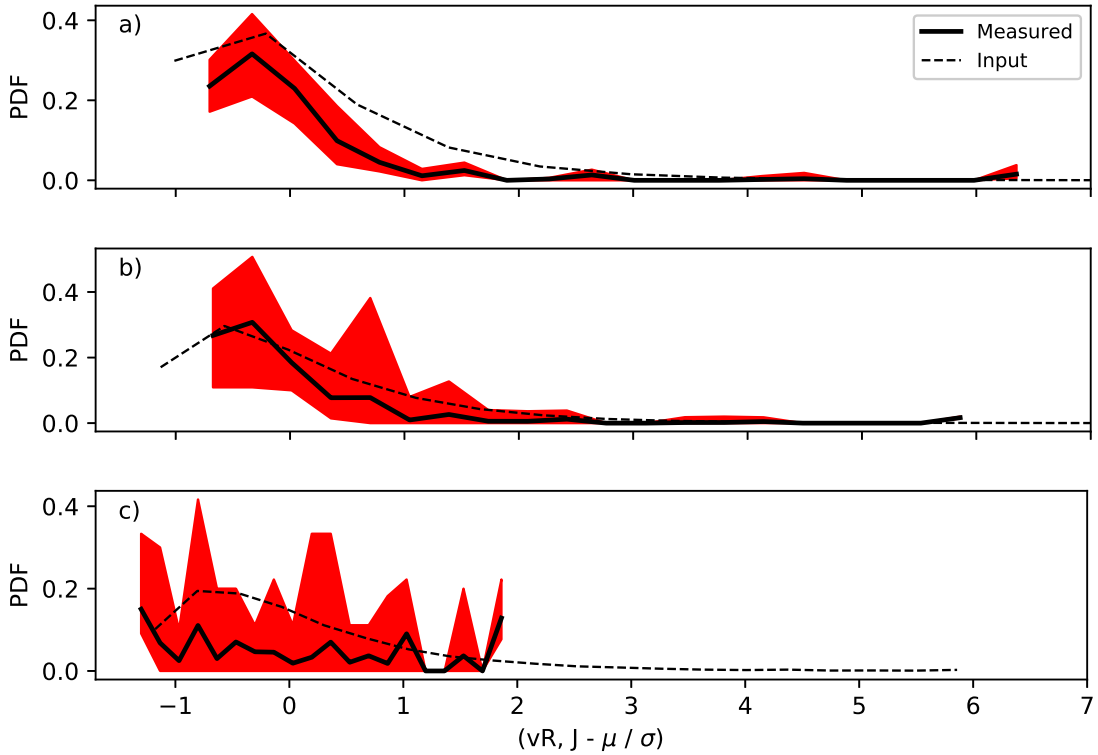

Figure 4: The black dashed line is the average input radial velocity PDF, the black solid line is the average measured radial velocity PDF with the red shaded area as the maxima and minima. Top to bottom is (a) low, (b) medium, and (c) high.

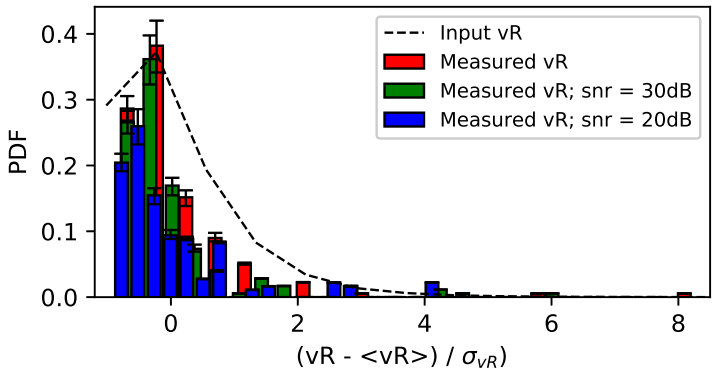

Figure 5: The radial velocity PDFs measured with no added noise in red, a signal to noise ratio of 30dB in green and 20dB in blue, with the input radial velocity PDF as the black line as reference.

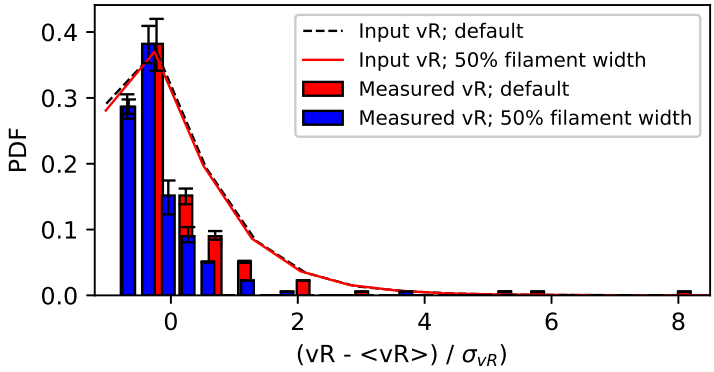

Figure 6: The input radial velocity distributions are the black dashed and red solid lines for the default and 50% reduced filament widths, respectively. The red bars are the default radial velocity case with the blue bars as the reduced filament width case.

a poloidal separation for all probes of 10mm and a 10mm radial offset for the radial probe. Here we tested 5mm poloidal and 5mm radial, 5mm poloidal and 10mm radial, 15mm poloidal and 15mm radial and finally we reversed the order of the probes in the default case of 10mm. From figure 7 we can see that the default case matches closest to the input distribution detecting 182 peaks, with the other 15mm case (161 peaks detected) following the shape of the distribution without matching the amplitude. The 5mm cases (183 peaks for (a), 181 peaks for (b)) arguably align with the general trend of the input but would not be definitive without a priori knowledge. The reversed case (204 peaks detected) follows the input distribution well, however, has a much larger amplitude spike than the default case. Figure 8 compares each measured case with the poloidal and radial 5mm case input distribution. For the probe separation test cases, we used a low intermittency and kept all the parameters identical other than the probe positions.

5. Discussion

The velocity technique investigated here resolves the radial velocity distribution reasonably well shows to work well in low intermittency cases as more filament peaks are detected allowing a larger statistical sample population. The technique works with with a signal to noise ratio of 30dB and 20dB, which are typical noise levels for these kinds of measurements. A reduced filament size does not seem to affect the ability to make measurements for the default probe spacing, however it may be likely small filaments combined with a large probe separation would reduce the number of filaments detected. The technique appears optimised with the default 10mm separation poloidally and radially, this may be due to the typical filament width which the default for our MO model simulations is 5-20mm. For separations of 5mm the total poloidal span is 10mm, which may struggle to detect some of the larger filaments across all three probes

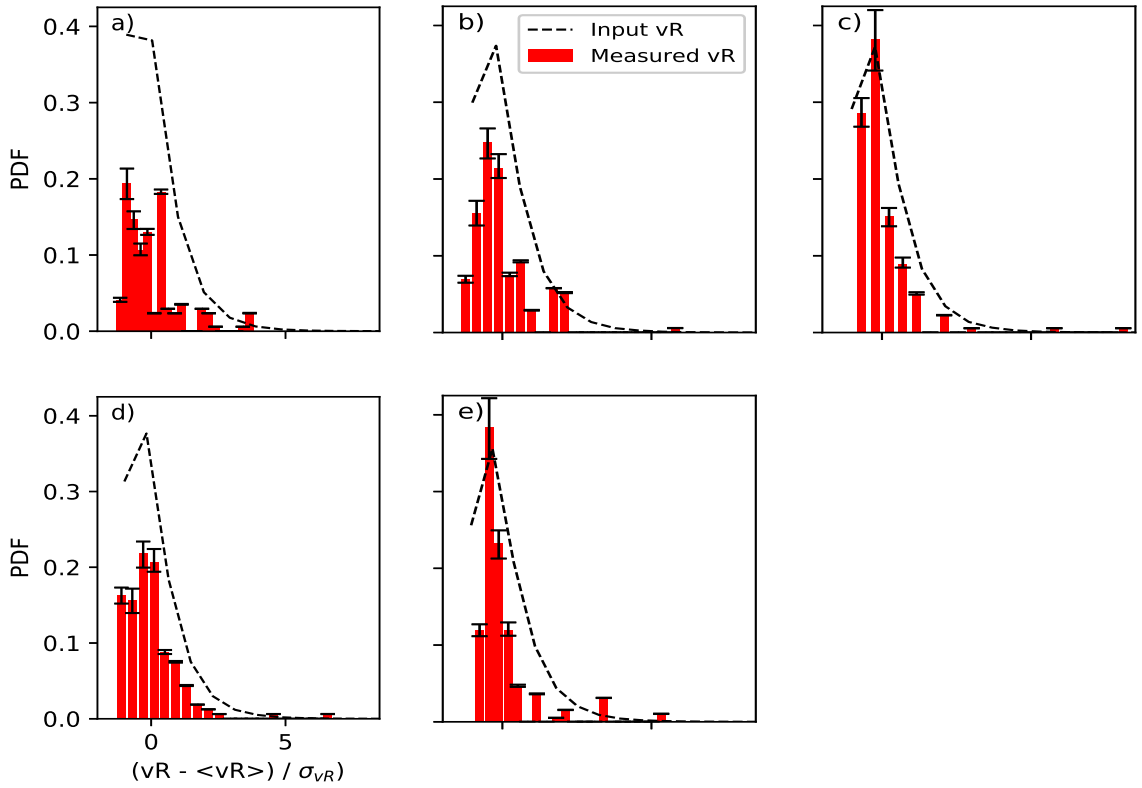

Figure 7: The black dashed line is the input radial velocity, and the red bars are the measured radial velocity for each case. From left to right on the top are (a) the poloidal 5mm and radial 5mm separation, (b) poloidal 5mm and radial 10mm case, and (c) the default 10mm poloidal and radial separations. Bottom left (d) is the 15mm poloidal and radial case, and (e) the bottom centre is the reversed probe order with the default probe separations.

especially for any filaments that do not have purely poloidal velocities as was discussed by Carralero et al [17] who had to compensate for this to avoid unrealistic results as their probes were spaced 5.5mm poloidally and 4mm radially. The 10mm cases have a poloidal span of 20mm the upper bound of the filament width and so are able to capture more filaments across all three probes. The 15mm case has a much greater poloidal span of 30mm however a 15mm separation of the probes may allow smaller filaments to pass between probes. The reversed probe layout with a spacing of 10mm matches the input profile well to an extent, other than the amplitude spike, this may be due to statistical anomaly or a mismatching of filament peaks across the probes. Averaging over several runs would most likely smooth out such anomalous amplitudes.

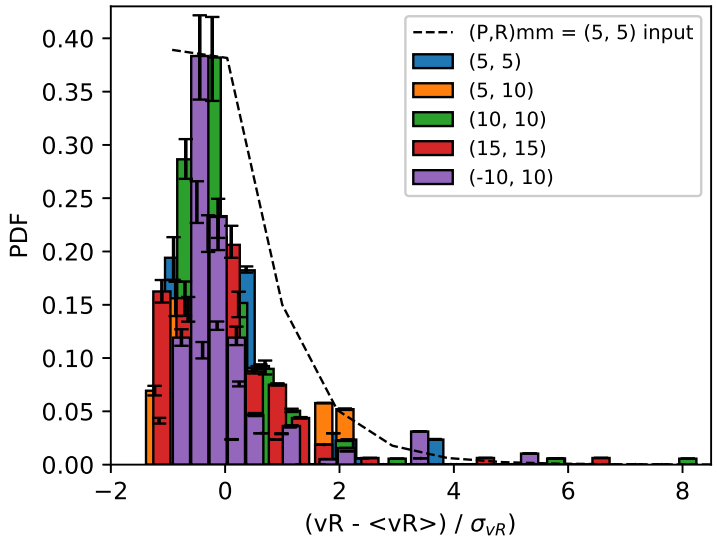

Figure 8: Measured radial velocity PDFs for different pin positions: black dashed line is the input PDF, blue is the 5mm case, orange is the 5mm poloidal and 10mm radial separation. green is the default 10mm case, red is the 15mm case and purple is the reversed probe order case

6. Conclusions

Once developed the new turbulence probe will be utilised in MAST-U on the midplane RP system to study the upstream filament dynamics, then, on the divertor RP system when it comes online to examine filament dynamics and provide comparison. The Langmuir probe diagnostic technique discussed in this paper for measuring the radial velocity distribution shows some promising preliminary simulation results. The technique performs well in low intermittency situations due to higher statistical resolution, and a probe spacing of 10mm appears to work well with the filament widths expected. With longer timescales and more detected filaments, this method will give capability to investigate the impact of the Super-X divertor on filamentary transport. We also aim to explore some of the other common probe techniques like conditional averaging, cross-correlation, calculating the average non-filament density, average filament density, and the autocorrelation time, from which we can use as an alternative method to calculate the radial velocity for comparison with the presented technique [13, 17, 21, 26]. Thus, adding further depth and understanding to our results in assessing filament properties.

Acknowledgments

The authors would like to thank Dr John Omotani for his thorough readthrough and helpful comments for this manuscript. This work has been carried out within the

framework of the EUROfusion Consortium and has received funding from the Euratom research and training programme 2014-2018 and 2019-2020 under grant agreement No 633053. The views and opinions expressed herein do not necessarily reflect those of the European Commission.

References

[1] Morris W, Harrison J R, Kirk A, Lipschultz B, Militello F, Moulton D and Walkden N R 2018 *IEEE Transactions on Plasma Science* **46** 1217–1226 URL https://doi.org/10.1109/TPS.2018.2815283

[2] Harrison J, Akers R, Allan S, Allcock J, Allen J, Appel L, Barnes M, Ayed N B, Boeglin W, Bowman C, Bradley J, Browning P, Bryant P, Carr M, Cecconello M, Challis C, Chapman S, Chapman I, Colyer G, Conroy S, Conway N, Cox M, Cunningham G, Dendy R, Dorland W, Dudson B, Easy L, Elmore S, Farley T, Feng X, Field A, Fil A, Fishpool G, Fitzgerald M, Flesch K, Fox M, Frerichs H, Gadgil S, Gahle D, Garzotti L, Ghim Y C, Gibson S, Gibson K, Hall S, Ham C, Heiberg N, Henderson S, Highcock E, Hnat B, Howard J, Huang J, Irvine S, Jacobsen A, Jones O, Katramados I, Keeling D, Kirk A, Klimek I, Kogan L, Leland J, Lipschultz B, Lloyd B, Lovell J, Madsen B, Marshall O, Martin R, McArdle G, McClements K, McMillan B, Meakins A, Meyer H, Militello F, Milnes J, Mordijck S, Morris A, Moulton D, Muir D, Mukhi K, Murphy-Sugrue S, Myatra O, Naylor G, Naylor P, Newton S, O'Gorman T, Omotani J, O'Mullane M, Orchard S, Pamela S, Pangione L, Parra F, Perez R, Piron L, Price M, Reinke M, Riva F, Roach C, Robb D, Ryan D, Saarelma S, Salewski M, Scannell S, Schekochihin A, Schmitz O, Sharapov S, Sharples R, Silburn S, Smith S, Sperduti A, Stephen R, Thomas-Davies N, Thornton A, Turnyanskiy M, Valovič M, Wyk F V, Vann R, Walkden N, Waters I and and H W 2019 *Nuclear Fusion* **59** 112011 URL https://doi.org/10.1088/1741-4326/ab121c

[3] Kotschenreuther M, Valanju P M, Mahajan S M and Wiley J C 2007 *Physics of Plasmas* **14** 072502 URL https://doi.org/10.1063/1.2739422

[4] Valanju P M, Kotschenreuther M, Mahajan S M and Canik J 2009 *Physics of Plasmas* **16** 056110 URL https://doi.org/10.1063/1.3110984

[5] Havlíčková E, Harrison J, Lipschultz B, Fishpool G, Kirk A, Thornton A, Wischmeier M, Elmore S and Allan S 2015 *Plasma Physics and Controlled Fusion* **57** 115001 URL https://doi.org/10.1088/0741-3335/57/11/115001

[6] Ryutov D D 2007 *Physics of Plasmas* **14** 064502 URL https://doi.org/10.1063/1.2738399

[7] Krasheninnikov S I, Kukushkin A S and Pshenov A A 2016 *Physics of Plasmas* **23** 055602 URL https://doi.org/10.1063/1.4948273

[8] Thornton A J, Fishpool G, Kirk A and and 2015 *Plasma Physics and Controlled Fusion* **57** 115010 URL https://doi.org/10.1088/0741-3335/57/11/115010

[9] D'Ippolito D A, Myra J R and Zweben S J 2011 *Physics of Plasmas* **18** 060501 URL https://doi.org/10.1063/1.3594609

[10] Kočan M, Gennrich F P, Kendl A and and H W M 2012 *Plasma Physics and Controlled Fusion* **54** 085009 URL https://doi.org/10.1088/0741-3335/54/8/085009

[11] Militello F, Dudson B, Easy L, Kirk A and Naylor P 2017 *Plasma Physics and Controlled Fusion* **59** 125013 URL https://doi.org/10.1088/1361-6587/aa9252

[12] Militello F, Walkden N R, Farley T, Gracias W A, Olsen J, Riva F, Easy L, Fedorczak N, Lupelli I, Madsen J, Nielsen A H, Ricci P, Tamain P and Young J 2016 *Plasma Physics and Controlled Fusion* **58** 105002 URL https://doi.org/10.1088/0741-3335/58/10/105002

[13] Vianello N, Tsui C, Theiler C, Allan S, Boedo J, Labit B, Reimerdes H, Verhaegh K, Vijvers W, Walkden N, Costea S, Kovacic J, Ionita C, Naulin V, Nielsen A, Rasmussen J J, Schneider B, Schrittwieser R, Spolaore M, Carralero D, Madsen J, Lipschultz B, Militello F and and 2017 *Nuclear Fusion* **57** 116014 URL https://doi.org/10.1088/1741-4326/aa7db3

[14] Garcia O E, Pitts R A, Horacek J, Madsen J, Naulin V, Nielsen A H and Rasmussen J J 2007 *Plasma Physics and Controlled Fusion* **49** B47–B57 URL https://doi.org/10.1088/0741-3335/49/12b/s03

[15] Kirk A, Ayed N B, Counsell G, Dudson B, Eich T, Herrmann A, Koch B, Martin R, Meakins A, Saarelma S, Scannell R, Tallents S, Walsh M, Wilson H R and the MAST team 2006 *Plasma Physics and Controlled Fusion* **48** B433–B441 URL https://doi.org/10.1088/0741-3335/48/12b/s41

[16] Boedo J A, Rudakov D, Moyer R, Krasheninnikov S, Whyte D, McKee G, Tynan G, Schaffer M, Stangeby P, West P, Allen S, Evans T, Fonck R, Hollmann E, Leonard A, Mahdavi A, Porter G, Tillack M and Antar G 2001 *Physics of Plasmas* **8** 4826–4833 URL https://doi.org/10.1063/1.1406940

[17] Carralero D, Birkenmeier G, Müller H, Manz P, deMarne P, Müller S, Reimold F, Stroth U, Wischmeier M and and E W 2014 *Nuclear Fusion* **54** 123005 URL https://doi.org/10.1088/0029-5515/54/12/123005

[18] Tsui C K, Boedo J A, Myra J R, Duval B, Labit B, Theiler C, Vianello N, Vijvers W A J, Reimerdes H, Coda S, Février O, Harrison J R, Horacek J, Lipschultz B, Maurizio R, Nespoli F, Sheikh U, Verhaegh K and Walkden N 2018 *Physics of Plasmas* **25** 072506 URL https://doi.org/10.1063/1.5038019

[19] Ayed N B, Kirk A, Dudson B, Tallents S, Vann R G L and and H R W 2009 *Plasma Physics and Controlled Fusion* **51** 035016 URL https://doi.org/10.1088/0741-3335/51/3/035016

[20] Kirk A, Thornton A J, Harrison J R, Militello F and and N R W 2016 *Plasma Physics and Controlled Fusion* **58** 085008 URL https://doi.org/10.1088/0741-3335/58/8/085008

[21] Nold B, Conway G D, Happel T, Müller H W, Ramisch M, Rohde V and and U S 2010 *Plasma Physics and Controlled Fusion* **52** 065005 URL https://doi.org/10.1088/0741-3335/52/6/065005

[22] Terry J L, Zweben S J, Hallatschek K, LaBombard B, Maqueda R J, Bai B, Boswell C J, Greenwald M, Kopon D, Nevins W M, Pitcher C S, Rogers B N, Stotler D P and Xu X Q 2003 *Physics of Plasmas* **10** 1739–1747 URL https://doi.org/10.1063/1.1564090

[23] Carralero D, Artene S, Bernert M, Birkenmeier G, Faitsch M, Manz P, de Marne P, Stroth U, Wischmeier M, Wolfrum E and and 2018 *Nuclear Fusion* **58** 096015 URL https://doi.org/10.1088/1741-4326/aacb04

[24] Brooks J N, Allain J P and Rognlien T D 2006 *Physics of Plasmas* **13** 122502 URL https://doi.org/10.1063/1.2401610

[25] Wenninger R, Albanese R, Ambrosino R, Arbeiter F, Aubert J, Bachmann C, Barbato L, Barrett T, Beckers M, Biel W, Boccaccini L, Carralero D, Coster D, Eich T, Fasoli A, Federici G, Firdaouss M, Graves J, Horacek J, Kovari M, Lanthaler S, Loschiavo V, Lowry C, Lux H, Maddaluno G, Maviglia F, Mitteau R, Neu R, Pfefferle D, Schmid K, Siccinio M, Sieglin B, Silva C, Snicker A, Subba F, Varje J and Zohm H 2017 *Nuclear Fusion* **57** 046002 URL https://doi.org/10.1088/1741-4326/aa4fb4

[26] Theodorsen A, Garcia O E, Horacek J, Kube R and Pitts R A 2016 *Plasma Physics and Controlled Fusion* **58** 044006 URL https://doi.org/10.1088/0741-3335/58/4/044006

[27] Yang Y, Counsell G and The MAST team 2003 *Journal of Nuclear Materials* **313-316** 734–737 ISSN 0022-3115 plasma-Surface Interactions in Controlled Fusion Devices 15 URL https://doi.org/10.1016/S0022-3115(02)01574-X

[28] Tamain P, Kirk A, Nardon E, Dudson B and and B H 2010 *Plasma Physics and Controlled Fusion* **52** 075017 URL https://doi.org/10.1088/0741-3335/52/7/075017

[29] Walkden N R, Adamek J, Allan S, Dudson B D, Elmore S, Fishpool G, Harrison J, Kirk A and Komm M 2015 *Review of Scientific Instruments* **86** 023510 URL https://doi.org/10.1063/1.4908572

[30] Elmore S, Allan S Y, Kirk A, Fishpool G, Harrison J, Tamain P, Kočan M, Gaffka R, Stephen R and and J W B 2012 *Plasma Physics and Controlled Fusion* **54** 065001 URL

https://doi.org/10.1088/0741-3335/54/6/065001

[31] Allan S, Elmore S, Kirk A, Kočan M and Tamain P 2013 *Journal of Nuclear Materials* **438** S1192–S1195 ISSN 0022-3115 proceedings of the 20th International Conference on Plasma-Surface Interactions in Controlled Fusion Devices URL https://doi.org/10.1016/j.jnucmat.2013.01.263

[32] Garcia O E 2012 *Phys. Rev. Lett.* **108**(26) 265001 URL https://link.aps.org/doi/10.1103/PhysRevLett.108.265001

[33] Militello F and Omotani J 2016 *Nuclear Fusion* **56** 104004 URL https://doi.org/10.1088/0029-5515/56/10/104004

[34] Militello F and Omotani J T 2016 *Plasma Physics and Controlled Fusion* **58** 125004 URL https://doi.org/10.1088/0741-3335/58/12/125004

[35] Militello F, Farley T, Mukhi K, Walkden N and Omotani J T 2018 *Physics of Plasmas* **25** 056112 URL https://doi.org/10.1063/1.5017919

[36] Walkden N R, Wynn A, Militello F, Lipschultz B, Matthews G, Guillemaut C, Harrison J and and D M 2017 *Plasma Physics and Controlled Fusion* **59** 085009 URL https://doi.org/10.1088/1361-6587/aa7365

[37] Agostinetti P, Spolaore M, Brombin M, Cervaro V, Franchin L, Grulke O, Killer C, Martines E, Moresco M, Peruzzo S, Vianello N and Visentin M 2018 *IEEE Transactions on Plasma Science* **46** 1306–1311 URL https://doi.org/10.1109/TPS.2018.2799638

[38] Kube R, Garcia O, Theodorsen A, Kuang A, LaBombard B, Terry J and Brunner D 2019 *Nuclear Materials and Energy* **18** 193–200 URL https://doi.org/10.1016/j.nme.2018.11.021

[39] Myra J R, Russell D A and D'Ippolito D A 2006 *Physics of Plasmas* **13** 112502 URL https://doi.org/10.1063/1.2364858

[40] Easy L, Militello F, Omotani J, Walkden N R and Dudson B 2016 *Physics of Plasmas* **23** 012512 URL https://doi.org/10.1063/1.4940330

[41] Vianello N, Carralero D, Tsui C, Naulin V, Agostini M, Cziegler I, Labit B, Theiler C, Wolfrum E, Aguiam D, Allan S, Bernert M, Boedo J, Costea S, Oliveira H D, Fevrier O, Galdon-Quiroga J, Grenfell G, Hakola A, Ionita C, Isliker H, Karpushov A, Kovacic J, Lipschultz B, Maurizio R, McClements K, Militello F, Nielsen A, Olsen J, Rasmussen J, Ravensbergen T, Reimerdes H, Schneider B, Schrittwieser R, Seliunin E, Spolaore M, Verhaegh K, Vicente J, Walkden N, Zhang W, and and 2019 *Nuclear Fusion* **60** 016001 URL https://doi.org/10.1088/1741-4326/ab423e

[42] Dudson B D, Ayed N B, Kirk A, Wilson H R, Counsell G, Xu X, Umansky M, Snyder P B and and B L 2008 *Plasma Physics and Controlled Fusion* **50** 124012 URL https://doi.org/10.1088/0741-3335/50/12/124012

[43] Garcia O, Horacek J and Pitts R 2015 *Nuclear Fusion* **55** 062002 URL https://doi.org/10.1088/0029-5515/55/6/062002